Supplemental Document:
Polarimetric iToF: Measuring High-Fidelity Depth through Scattering Media

Daniel S. Jeon[†] Andréas Meuleman[†] Seung-Hwan Baek[*] Min H. Kim[†]

[†] KAIST [*] POSTECH

In this Supplemental Document, we provide details of the analytic solution about the amplitude estimation of unpolarized backscattered light. We also additional discussion, results and comparisons.

1. Amplitude Estimation

For completeness, we start by rewriting Equation (16) in the main paper here:

$$\left\|a^{\perp}\exp(\mathrm{i}\varphi^{\perp}) - \overline{a}_S^u \exp(\mathrm{i}\overline{\varphi}_S^u)\right\| - k_0 s^{\perp} + \frac{\overline{a}_S^u \int_{\varphi_0}^{\infty} a_S^u(\varphi) d\varphi}{\left\|\int_{\varphi_0}^{\infty} a_S^u(\varphi)\exp(\mathrm{i}\varphi) d\varphi\right\|} = 0. \tag{1}$$

We can further expand this using the Euler equation as:

$$\left(a^{\perp}\cos\left(\varphi^{\perp}\right) - \overline{a}_S^u \cos\left(\overline{\varphi}_S^u\right)\right)^2 + \left(a^{\perp}\sin\left(\varphi^{\perp}\right) - \overline{a}_S^u \sin\left(\overline{\varphi}_S^u\right)\right)^2 - \left(k_0 s^{\perp} - \overline{a}_S^u \frac{k_0}{\overline{k}_S^u}\right)^2 = 0. \tag{2}$$

We then rearrange the formation with respect to the amplitude $\overline{a}_S^u$ as

$$\left(\overline{a}_S^u\right)^2 \left(1 - \left(\frac{k_0}{\overline{k}_S^u}\right)^2\right) - 2\overline{a}_S^u \left[a^{\perp}\left(\cos\left(\varphi^{\perp}\right)\cos\left(\overline{\varphi}_S^u\right) + \sin\left(\varphi^{\perp}\right)\sin\left(\overline{\varphi}_S^u\right)\right) - \frac{\left(k_0\right)^2}{\overline{k}_S^u} s^{\perp}\right] + \left(a^{\perp}\right)^2 - \left(k_0 s^{\perp}\right)^2. \tag{3}$$

Note that Equation (3) is the quadratic equation for the amplitude $\overline{a}_S^u$. The solution for the quadratic equation is given as

$$\begin{aligned}
\overline{a}_S^u &= \frac{c_2 + \sqrt{c_2^2 - c_1 c_3}}{c_1}, \text{where} \\
c_1 &= \left(1 - \left(\frac{k_0}{\overline{k}_S^u}\right)^2\right), \\
c_2 &= \left[a^{\perp}\left(\cos\left(\varphi^{\perp}\right)\cos\left(\overline{\varphi}_S^u\right) + \sin\left(\varphi^{\perp}\right)\sin\left(\overline{\varphi}_S^u\right)\right) - \frac{\left(k_0\right)^2}{\overline{k}_S^u} s^{\perp}\right], \\
c_3 &= \left(a^{\perp}\right)^2 - \left(k_0 s^{\perp}\right)^2.
\end{aligned} \tag{4}$$

2. Calibration of Scalar α

While the extinction coefficients σ, σ_i, and σ_p in our model depend on the fog density, the scalar α is independent of the density. Rather, the scalar α has a dependency in terms of spatial locations, resulting in per-pixel α. To obtain the spatially-varying α, we built a closed chamber where a fog generator creates fog. We then wait for the fog to stabilize within the box physically and capture the foggy scene without objects in order to calibrate the scalar α.

3. Discussions

3.1. Optically-thin Scattering Media

There are a couple of assumptions that our method is based on. First, we assume that diffuse polarization from the surface is weak enough to be negligible $T_{\phi}^{p} \approx 0$ through multiple scattering. Second, we assume that light transport occurs through optically thin scattering media, i.e., light scattering reflected from the target surfaces is negligible.

3.2. Fog Homogeneity Assumption

In the real-world imaging scenario, a participating medium may consist of heterogeneous particles. However, it is too challenging to formulate the entire interaction among heterogeneous participating particles in an analytical form. To keep the fog estimation problem tractable, we assume the homogeneity of the participating medium, focusing on depth estimation.

3.3. 2π Ambiguity

Indirect ToF can estimate with a phase range from 0 to 2π. A phase over 2π is wrapped by 2π, which limits the depth estimation range. The depth limit within a single wrapping count is defined as $\frac{c}{2f}$, where c is the speed of light in the operating medium, and f is the modulation frequency. Hence, the depth limit can be extended by choosing a lower frequency f for light modulation as long as the sensor's dynamic range allows. In practice, for active i-ToF imaging, the maximum depth range is usually limited by the power of the light source rather than the wrapping distance, so we assume that the wrapping problem is not critical for our application. Moreover, the MHz modulation frequencies used in typical iToF cameras present a small number of phase wraps which can be estimated in a robust manner using a variant of the Chinese remainder theorem.

3.4. Spatial Regularization

Our main scope is to devise a polarized phasor model for the indirect ToF in scattering media and solve the model analytically to estimate the depth from each pixel's phasor observation. This method is directly applicable to each pixel independently. Our estimated depth may present noise, which could be improved by plugging in an additional process, such as adding a regularization term when computing the extinction coefficient for each pixel or applying smoothing algorithms such as a guided filter. Developing an efficient depth denoising algorithm and phase-reconstruction method would be interesting for future work.

3.5. Assumption of random polarization

As the skylight is partially polarized depending on the angle between the sun and the observer, i.e., near grazing angles, polarized scattering occurs in nature. Also, it can be modeled using a deterministic scattering model of polarization. However, in our experimental setup, the camera and the active illumination are placed next to each other, looking in the same direction. In this coaxial optics setup, such deterministic scattering rarely occurs. Random polarization tends to occur through retro-reflection. To our knowledge, the proposed model may not be applicable to the deterministic scattering of polarized light.

4. Additional Results

Here, we provide additional qualitative results, comparison, and evaluations.

4.1. Subsurface scattering and sparse k-bounce interference

We aim to capture opaque objects under scattering media, which commonly occurs in practical applications such as autonomous driving under fog and underwater navigation. We thus design our method with an assumption that the TOF phase continuously decreases within the environment. It would be an interesting future work to extend our method to handle sparse k-bounce multi-path and diffuse subsurface scattering. This is revealed in our experiment of capturing a convex V-groove object under fog. Our method achieves higher depth accuracy compared to the naive ToF imaging from the RMSE depth error of 2.39 cm to 0.61 cm, the estimated inner angle of the V-groove is 97.56°, which deviates from the ground-truth 90°, due to sparse k-bounce multipath interference.

4.2. Comparison

Figures 1, 2, and 3 show our results on varying fog densities compared to parallel- and cross-polarization imaging, where our method outperforms the baselines. Figures 4, 5, 6, 7, and 8 demonstrate that our method outperforms the state-of-the-art ToF imaging methods developed for scattering environments.

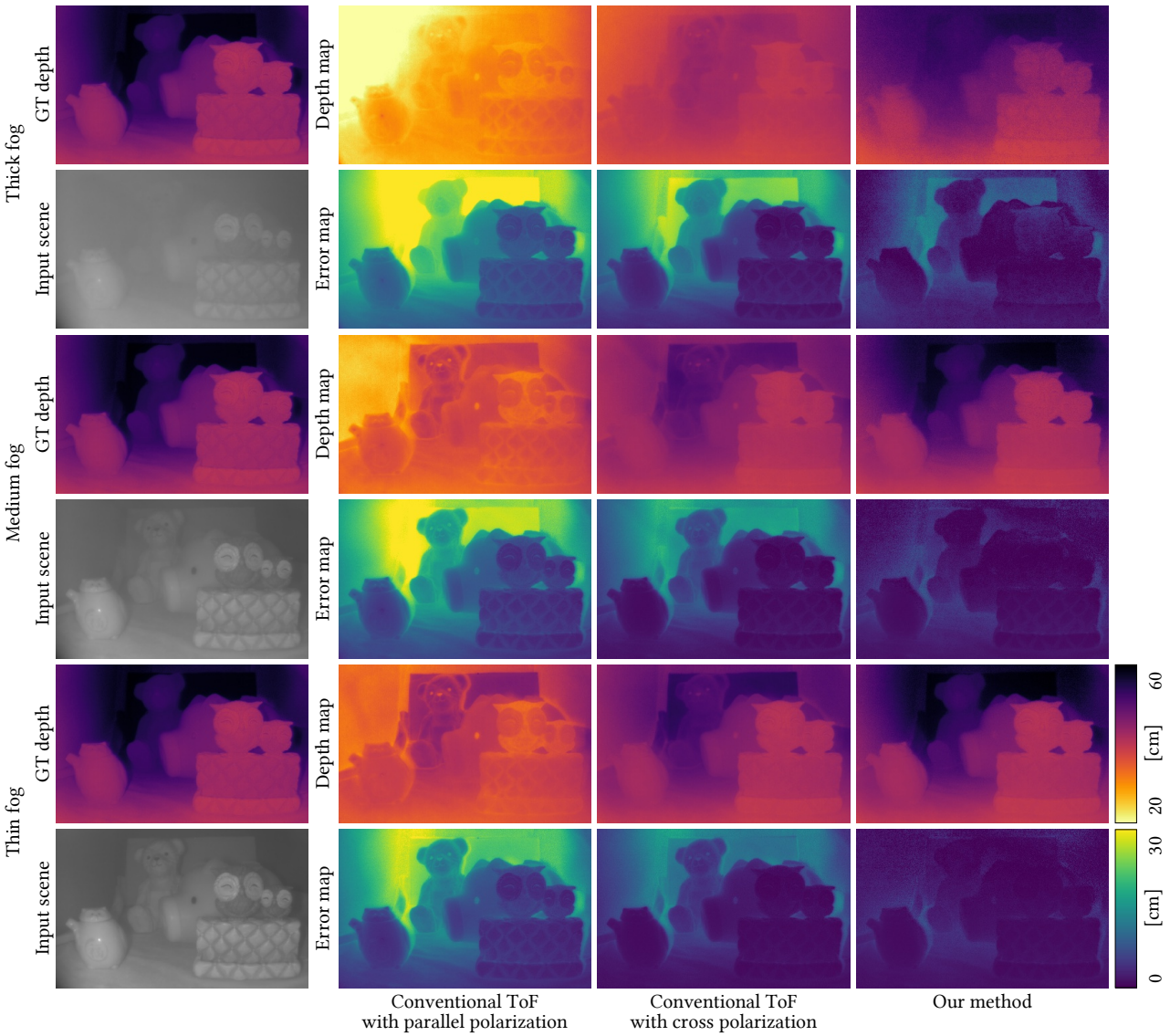

Figure 1. *Scene: Bear and Owl.* Our method successfully estimates accurate depth for varying degree of fog densities. Note that conventional ToF methods with parallel- and cross-polarization configurations fail to handle the scattering effect.

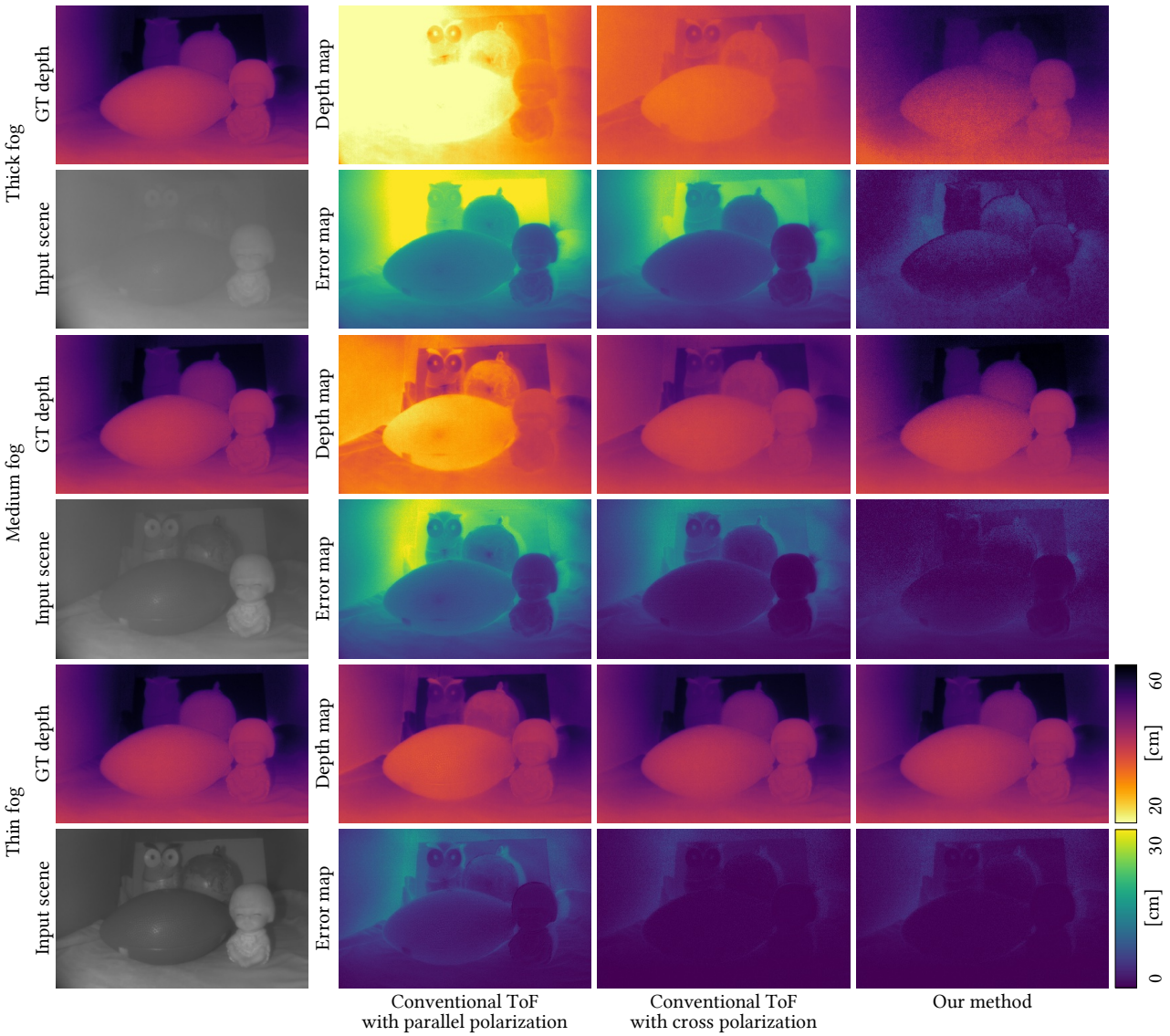

Figure 2. *Scene: Ball and Earth.* Our method successfully estimates accurate depth for varying degree of fog densities. Note that conventional ToF methods with parallel- and cross-polarization configurations fail to handle the scattering effect.

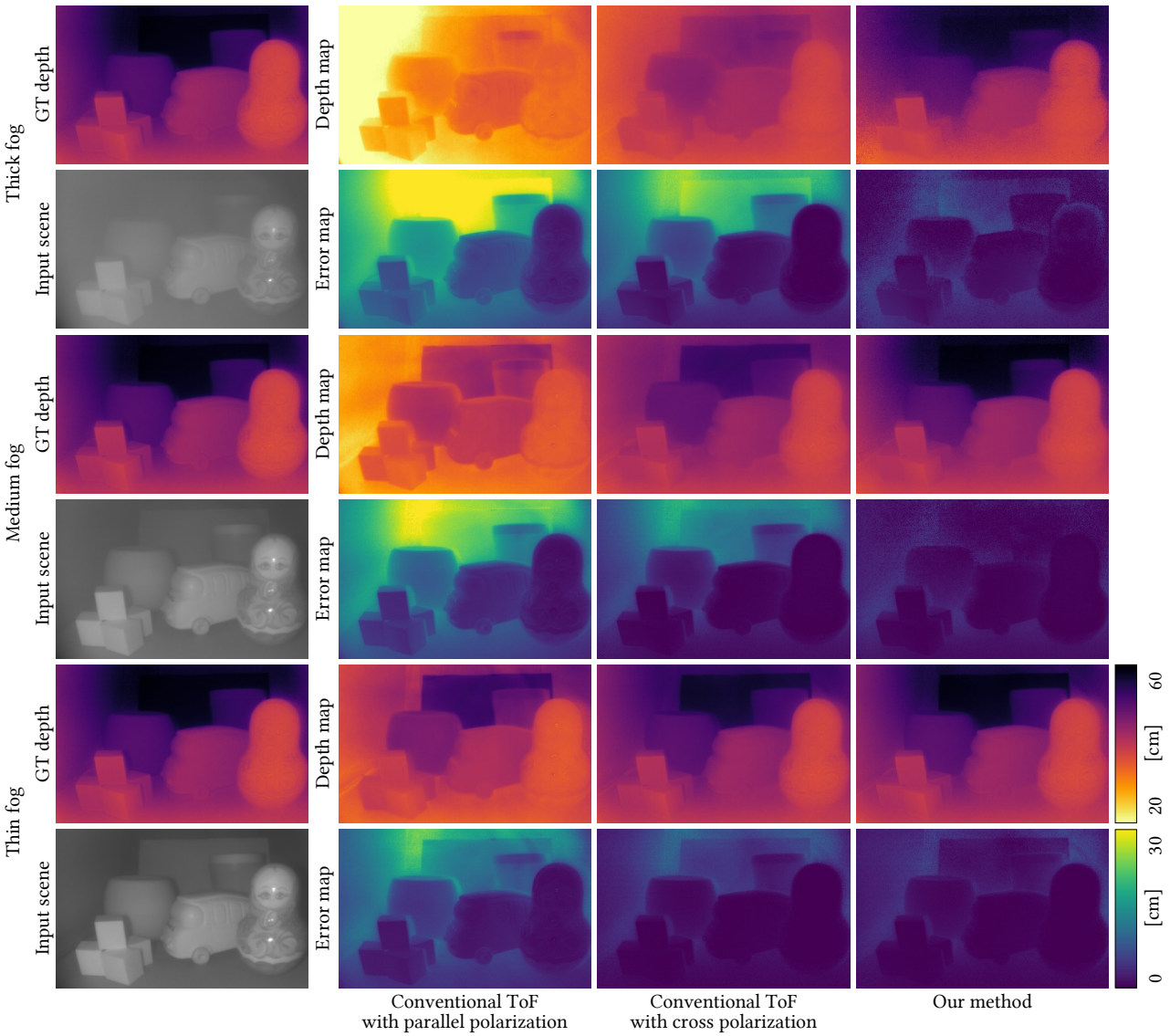

Figure 3. *Scene: Doll and Block.* Our method successfully estimates accurate depth for varying the degree of fog densities. Note that conventional ToF methods with parallel- and cross-polarization configurations fail to handle the scattering effect.

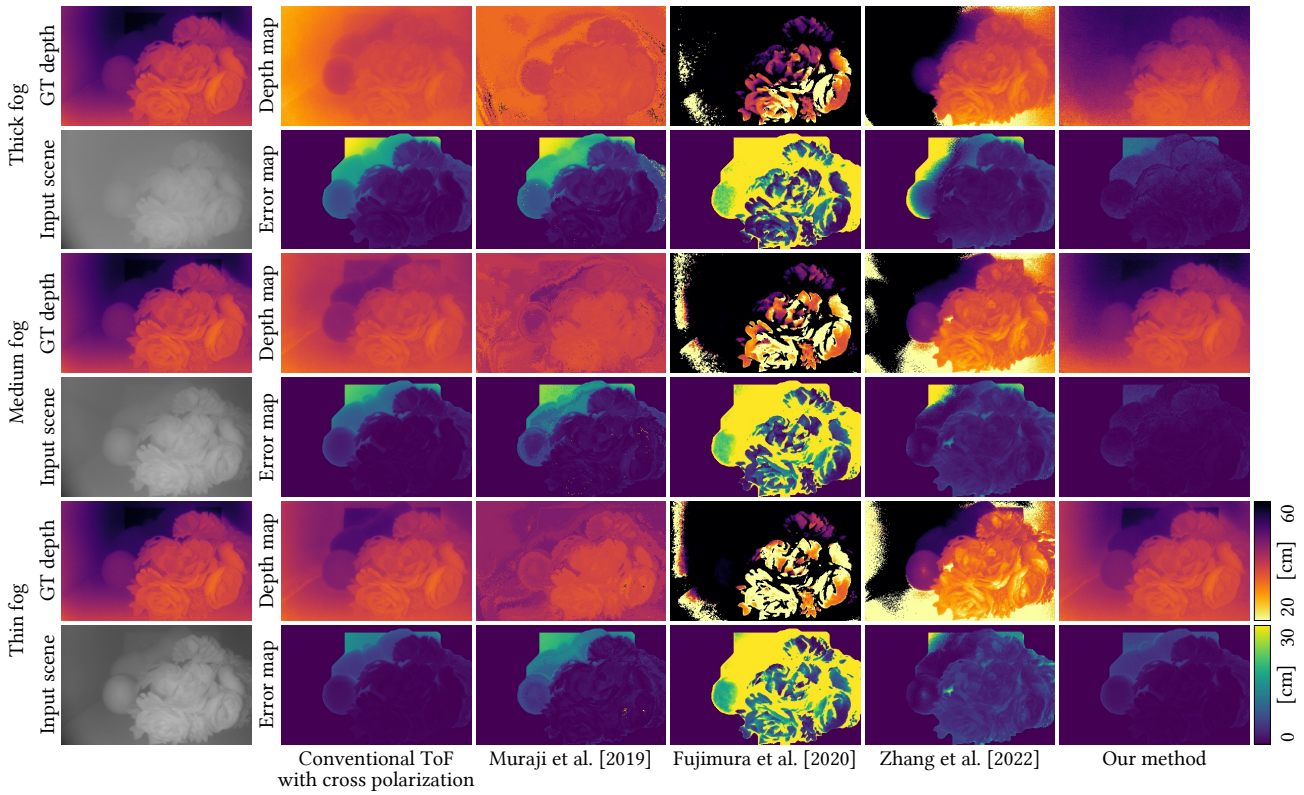

Figure 4. *Scene: Flower and Orange.* We compare our method to state-of-the-art ToF methods for scattering environments. We outperform all the compared methods.

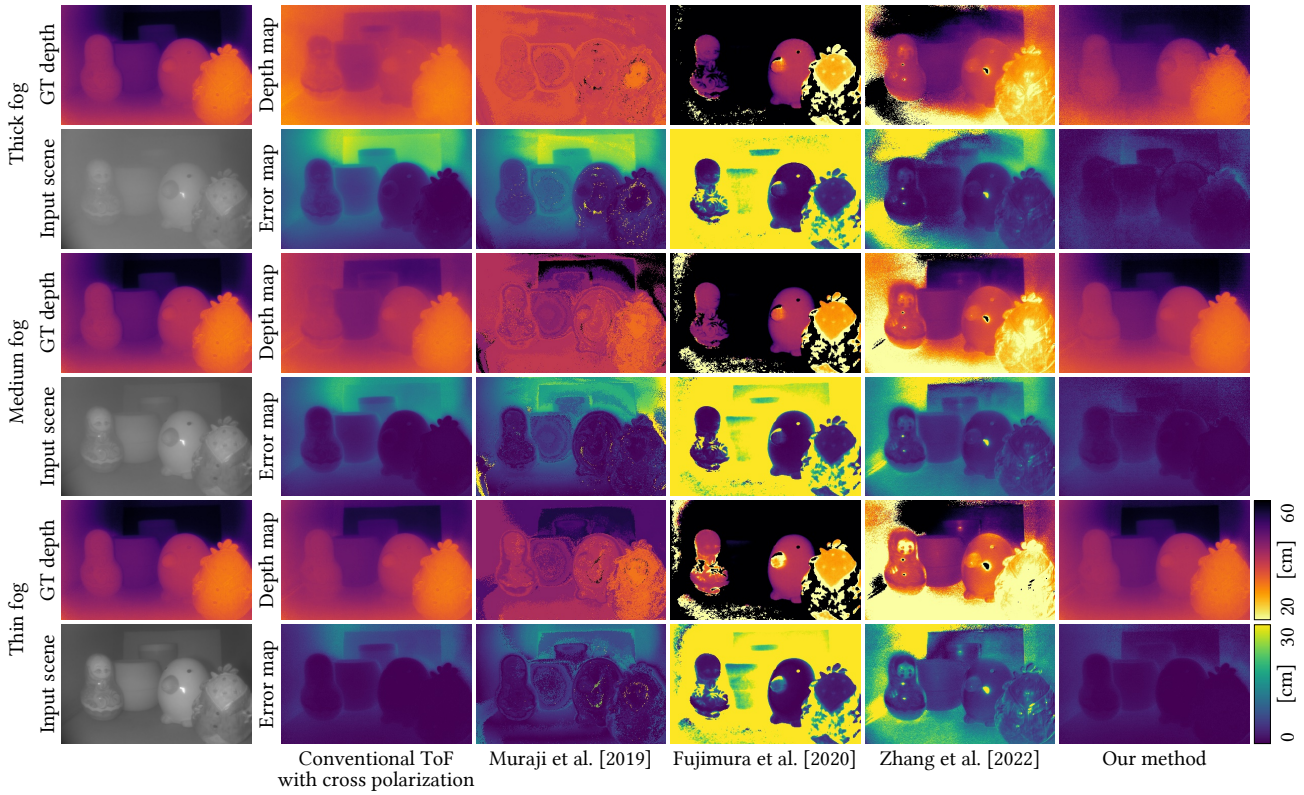

Figure 5. *Scene: Duck.* We additionally compare our method to state-of-the-art ToF methods for scattering environments.

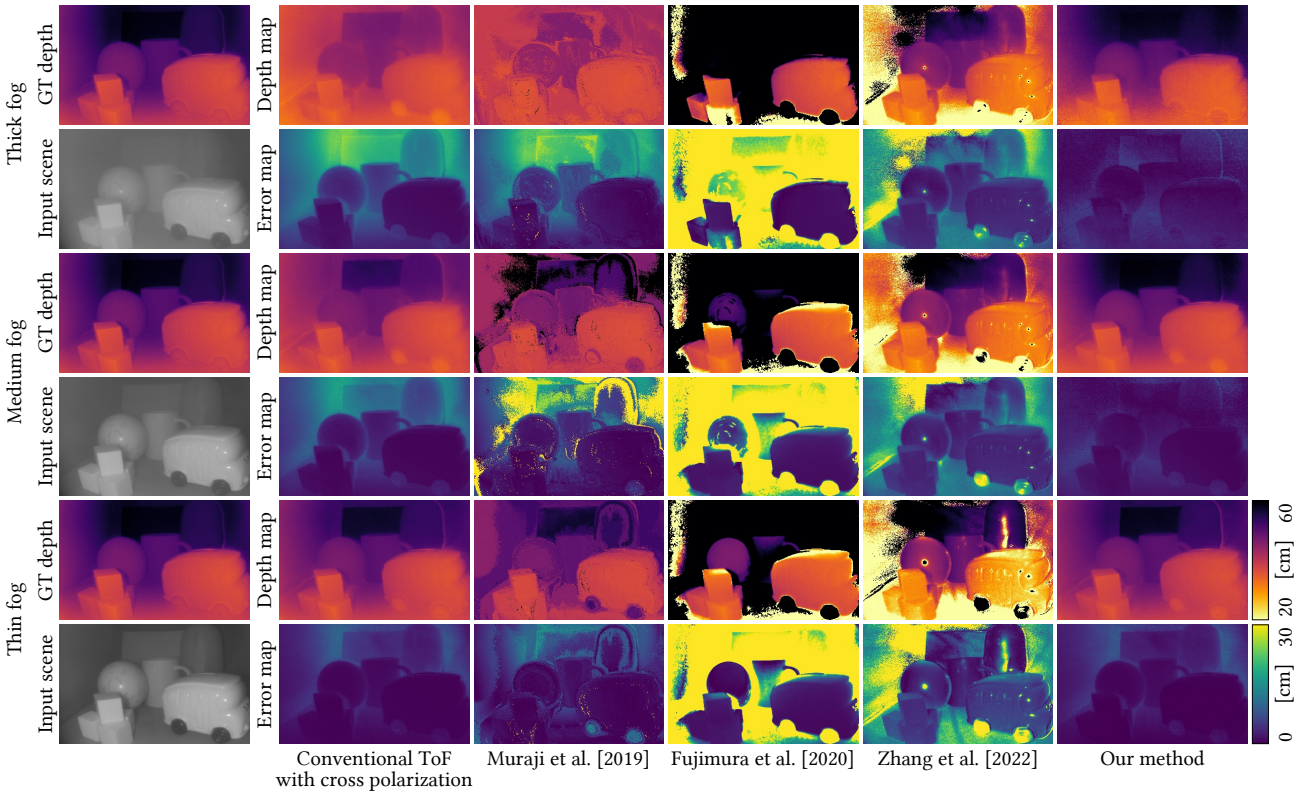

Figure 6. *Scene: Bus and Earth.* We additionally compare our method to state-of-the-art ToF methods for scattering environments.

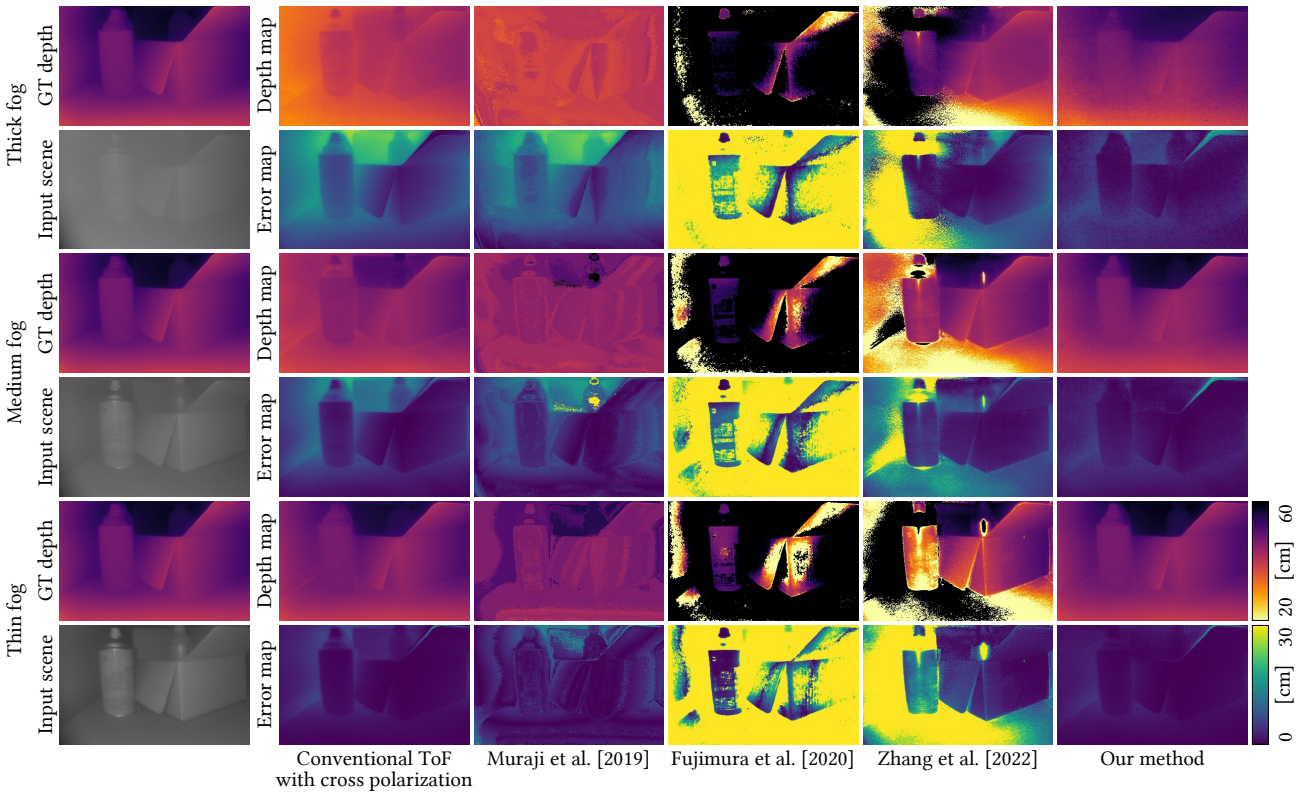

Figure 7. *Scene: Box and Can.* We additionally compare our method to state-of-the-art ToF methods for scattering environments.

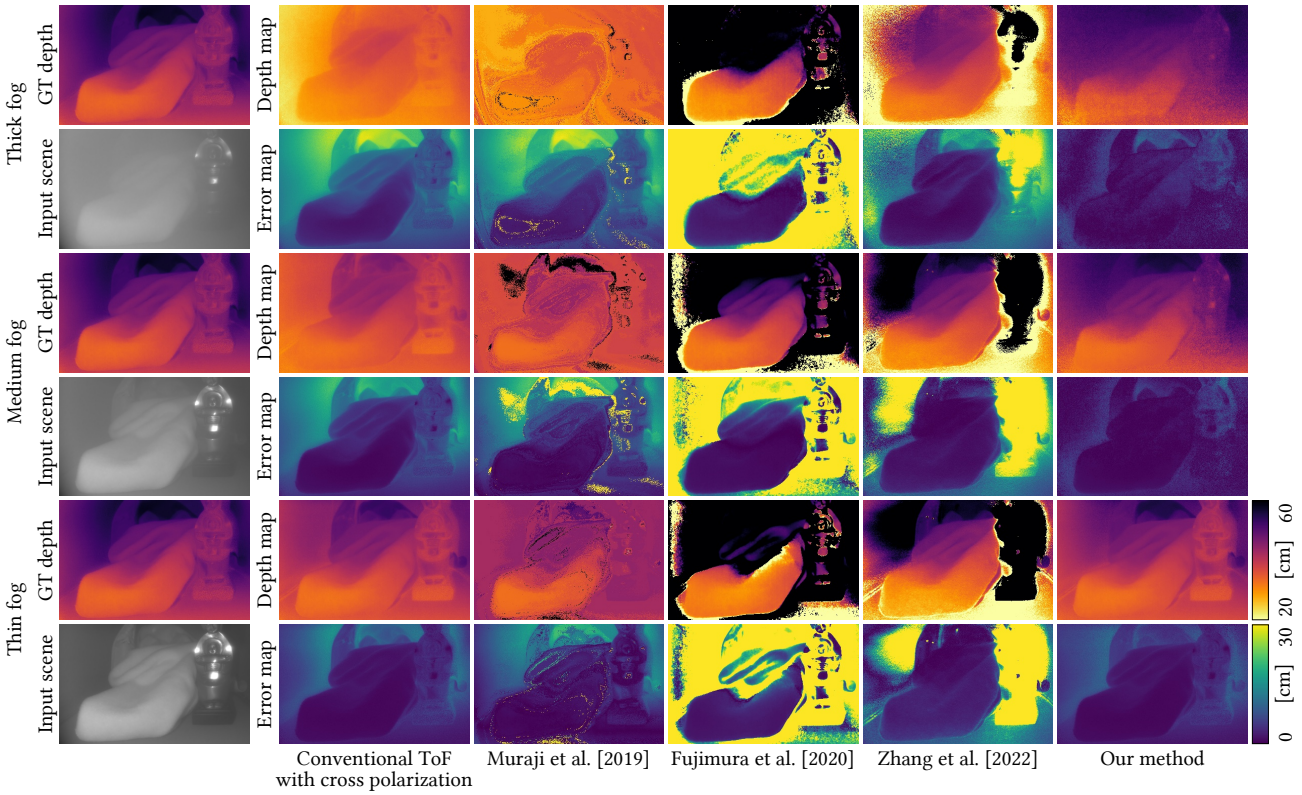

Figure 8. *Scene: Cloth and Statue.* We additionally compare our method to state-of-the-art ToF methods for scattering environments.

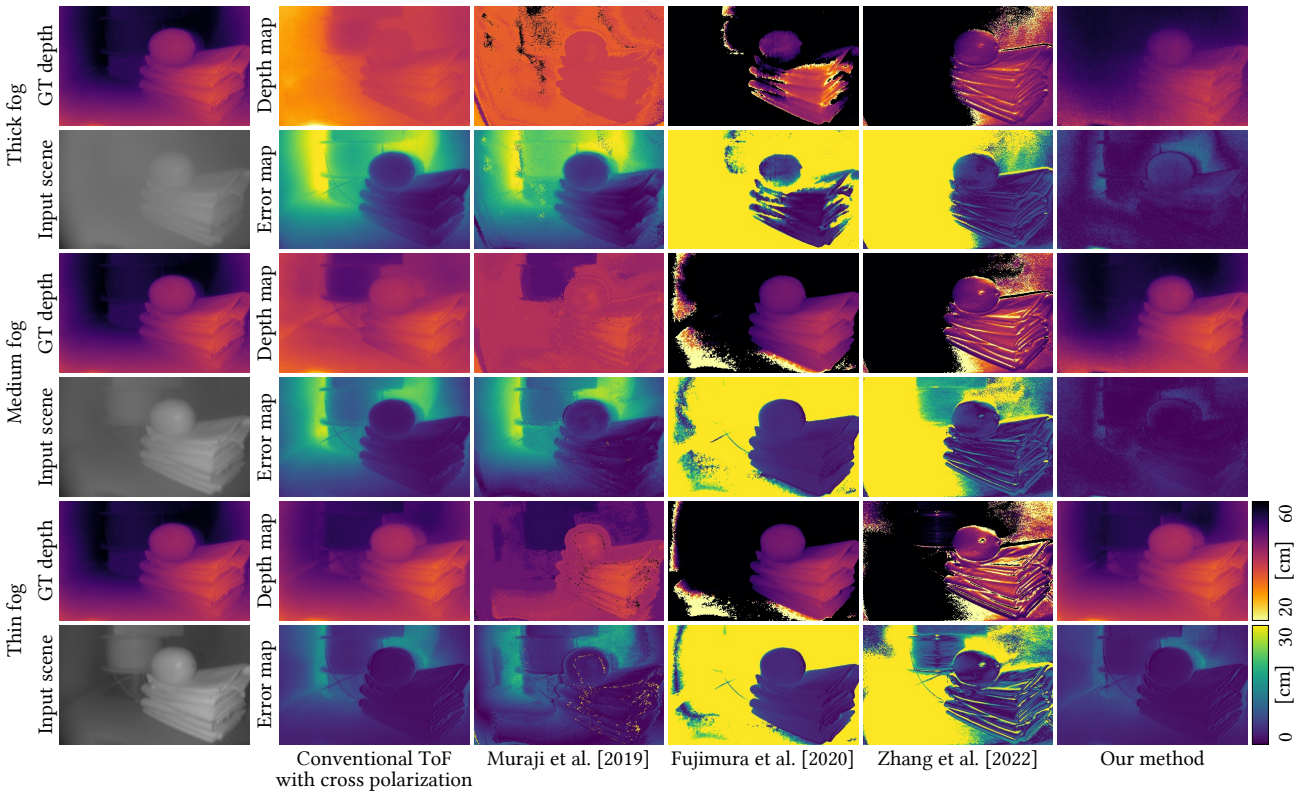

Figure 9. *Scene: Filament and Cloth.* We additionally compare our method to state-of-the-art ToF methods for scattering environments.

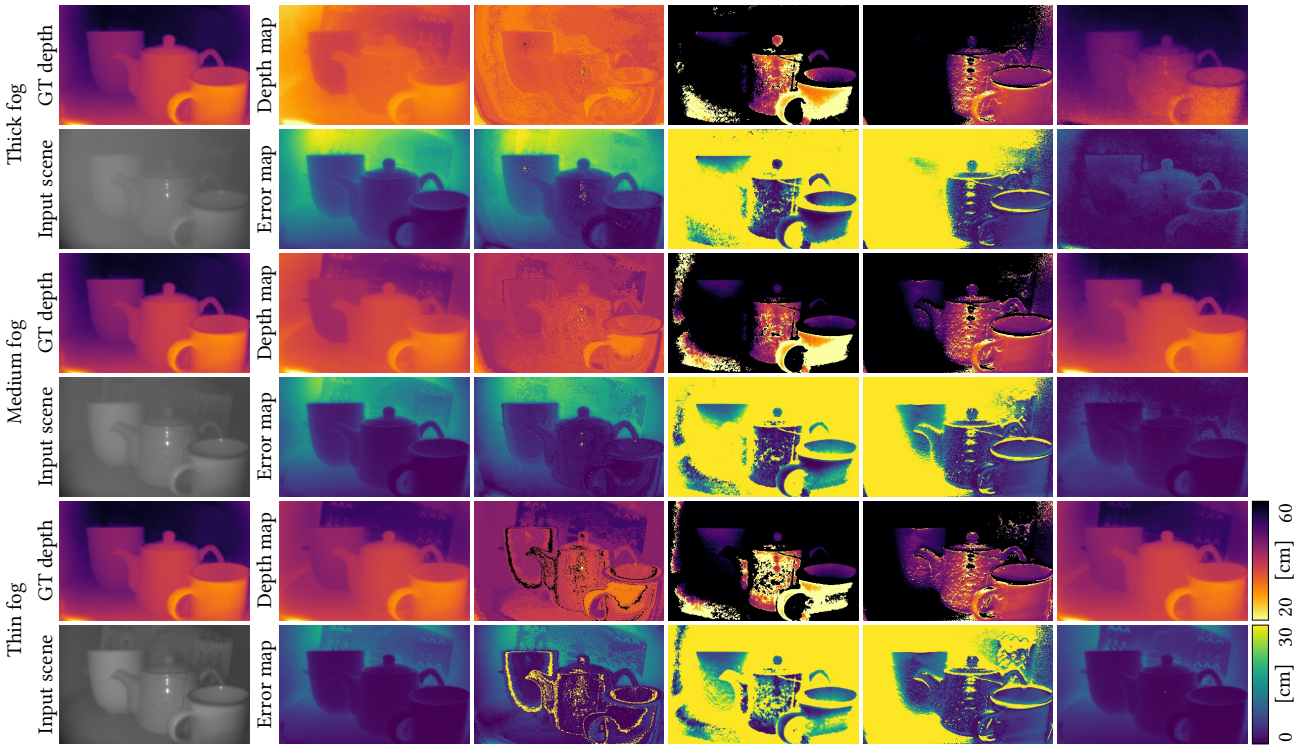

Figure 10. *Scene: Cups.* We additionally compare our method to state-of-the-art ToF methods for scattering environments.